Distance magnetic nanoparticle detection using a magnetoelectric sensor for clinical interventions

D. T. Huong Giang, D. X. Dang, N. X. Toan, N. V. Tuan, A. T. Phung, and N. H. Duc

Distance magnetic nanoparticle detection using a magnetoelectric sensor for clinical interventions

D. T. Huong Giang,[1,a)] D. X. Dang,[1] N. X. Toan,[1] N. V. Tuan,[2] A. T. Phung,[3] and N. H. Duc[1,a)]

[1]*Laboratory for Micro-Nano Technologies and Faculty of Engineering Physics and Nanotechnology,*
VNU University of Engineering and Technology, Vietnam National University, Hanoi,
144 Xuan Thuy Road, Cau Giay, Hanoi, Vietnam
[2]*Department of Physics, Le Quy Don University, 236 Hoang Quoc Viet Road, Cau Giay, Hanoi, Vietnam*
[3]*Departement of Electrical and Electronic Equipment, School of Electrical Engineering, Hanoi University*
of Science and Technology, Suite 106, C3 Building, 1 Dai Co Viet Road, Hanoi, Vietnam

Distance magnetic nanoparticle detections were investigated by using a magnetoelectric based magnetic sensor with a long type bilayer Metglas/PZT laminate composite. In homogeneous magnetic fields, the sensor exhibits a sensitivity of 307.4 mV/Oe, which is possible for a detection limit of 2.7×10^{-7} emu. This sensor can detect an amount of 0.31 μg of the superparamagnetic Fe_3O_4-chitosan fluid at 2 mm height above the sensor surface. To detect a spot with magnetic nanoparticles at a distance of about 7.6 mm, it should contain at least 50 μg of iron oxide. This approach can develop the local detection of magnetic nanoparticles at a depth of centimeters in the body during clinical interventions. *Published by AIP Publishing.* [http://dx.doi.org/10.1063/1.4973729]

I. INTRODUCTION

Detections of magnetic microbeads or nanoparticles have been strongly developed for biomedical applications. In biochip applications, the magnetic microbeads or nanoparticles labeled with biomolecules (proteins, DNA, etc.) are employed in detecting target biomolecules by binding the probe biomolecules immobilized on the magnetic sensing surface. For these cases, magnetic sensing micro-bioassays have been developed on the basis of giant magnetoresistive (GMR), planar Hall effect (PHE), semiconductor Hall, and anisotropic magnetoresistive ring (AMR) sensors.[1,2] Among them, the PHE sensors exhibit the highest magnetic field sensitivity (of about 15 μV/Oe) and detection limit of 1.98 $\times 10^{-10}$ emu,[3,4] at which the distance between the particles and the sensor surface is of about 15 μm only. *In vivo* applications, magnetic nanoparticles (MNPs) usually locate in deep tissues. Thus, sensitive detections of magnetic nanoparticles at a long distance are required. Up to now, the clinical use of magnetic nanoparticles (MNPs) is mainly as a contrast agent in MRI. In the last decade, several studies have been published in medical applications of using the MNPs for sentinel lymph node biopsy (SLNB). In the clinical practice of SLNB detection, it is important to detect the MNPs at a substantial depth of several centimeters within maximally a few seconds.[5] For the case of the human breast, the maximum depth of a tumor falls between 0.7 and 3.6 cm. Hathaway *et al.* have demonstrated the ability to detect labeled breast cancer cells at a depth of 4.5 cm.[6] The present imaging system could detect an amount of 100 μg MNP sample located at a distance of 30 mm, and the signal-to-noise ratio as high as 5 has been reported.[7] Similarly, the non-invasive detection of blood pulse and flow velocity has received a lot of attention over the years.[8] By the same approach to detect the presence of magnetic particles near a sensor surface (at distance of some 10 μm to ml), it has been developed in DNA-labeled magnetic disposable cards[9] or microfluidic channels detection for biochip applications.[10,11] This is especially important in wash-free bioassay protocols,[12] which do not require the removal of particles from a sensor surface during measurements as conventional magnetic-particle-sensing methods.[13,14]

All of the above mentioned applications require the development of suitable probes that unambiguously detect the magnetic microbeads or nanoparticles not only on the magnetic sensing surface but also at a depth of several millimeters *in vivo* tracer. In this context, the magnetoelectric (ME) based magnetic sensor might be a suitable solution.

Indeed, highly sensitive magnetic field sensors can be obtained by using the ME composites with high ME coefficient. This technology competes with Hall probes. The ME effect directly transforms the magnetic field to the electrical field with high radiation and temperature stability. The working principle of magnetic sensing in the ME composites is simple and direct. It can be used for detecting both *ac* and *dc* fields.[15] In fact, small long-type ME laminates of Terfenol-D (or Metglas) and PZT reached a sensitivity better than 1 V/Oe, i.e., 10^5 times higher than that of the above mentioned planar Hall effect (PHE) sensors. Their detection limit is about 10^{-6} emu using a constant amplitude low frequency drive and can be enhanced to 10^{-8} emu under resonant drive[16] for several millimeter distance from the sensor surface.

The goal of this paper is to investigate the aspects of magnetic nanoparticles detection for a broad application range in biochip as well as clinical intervention. In Secs. II and III, the design, realization, and characteristics of a ME sensor, which enables remote distant detections of the stray field of magnetic nanoparticles, are given.

---

a)Authors to whom correspondence should be addressed. Electronic addresses: giangdth@vnu.edu.vn, Tel.: 84 4 3754 9665, Fax: 84 4 3754 7460 and ducnh@vnu.edu.vn, Tel.: 84 4 3754 9665, Fax: 84 4 3754 7460.

II. EXPERIMENTAL

A. ME sensor fabrication

The ME-based magnetic sensor was fabricated following the construction process reported earlier in Refs. 17–19. The ME laminate composite was formed by bonding an out-of-plane polarized piezoelectric 500 μm-thick PZT plate (APCC-855) of American Piezoceramics, Inc., PA, USA with 18 μm-thick soft magnetic Ni-based Metglas ribbon (Fig. 1(a)). The sensor dimension of 15 mm (in length) and 1 mm (in width) was used. Thanks to the shape anisotropy, this geometry supports approaching the maximal sensor sensitivity with the intrinsic magnetic softness of the Ni-based Metglas ribbon along its x-length and against sensing with vertical (z) magnetic fields. A solenoid coil (Fig. 1(b)) is wrapped around the ME composite laminate to generate an exited ac-magnetic field. The sensor is bonded to a printed circuit board (Fig. 1(c)) by using epoxy (Fig. 1(d)) and its final prototype is given in Fig. 1(e). The distance between the ME laminate and the sensor surface is 1 mm.

B. Sensor working principle

The well-known ME effect is observed in ME laminate composites (shown in Fig. 1(a)), thanks to the mechanical coupling between the components. Under in-plane applied *dc* magnetic fields H_{dc}, the PZT plate undergoes a forced strain which is induced by the magnetostrictive layers. The ME voltage response (V_{ME}) to this forced strain is subsequently induced across the thickness of the piezoelectric plate (t_{PZT}). In essence, the ME effect produces an electric dipole through the whole piezoelectric structure, so the net positive and negative charges appear on its opposite, outer faces. These parasitic charges and artifacts, however, easily disappear and need to be proceeded carefully. In the dynamic method, the phase sensitive technique using a lock-in amplifier is applied.[15] In this case, the principle for the appearance of the ME voltage, i.e., the principle for the H_{dc} signal detection can be recognized as follows: (i) First, a weak constant ac magnetic field h_{ac} ($= h_o \sin(2\pi f_o t)$) oscillating at the resonant frequency is used to excite the laminate into vibration along its length axis via the

FIG. 1. ME sensor construction: (a) Metglas/PZT composite with electrodes, (b) solenoid coil generating an ac-magnetic field, (c) printed circuit board, (d) packaged sensor using epoxy, and (e) sensor prototype.

attached solenoid coils. (ii) Then, small variations in H_{dc} are detected as small induced ME voltage changes. In this context, the lock-in amplifier simultaneously supplies an *ac* current to the solenoid, exciting the above mentioned oscillating field.

In the total applied magnetic fields $H = H_{dc} + h_{ac}$, the polarization process creates an electric field of the form $E = \alpha_E \cdot H$, where α_E ($= dE/dH = V_{ME}/h_{ac} \cdot t_{PZT}$) denotes the magnetoelectric voltage coefficient. As a result, the value of the ME voltage V_{ME} is derived as[15,17–19] $V_{ME} = \alpha_E \cdot h_{ac} \cdot t_{PZT}$, where α_E depends on the H_{dc} or on the sensor working point.

In applied magnetic fields H_{dc}, the magnetic nanoparticle is magnetized, becoming a magnetic dipole. In turn, it creates a dc stray field, which also serves the role of an additional dc magnetic field to H_{dc} and causes its contribution to the ME sensor signal.

The ME sensor signal V_{ME} was measured using a commercial DSP lock-in amplifier (Model 7265 of Signal Recovery). The noise bandwidth of 8.3375 Hz was used by setting the output time constant to 20 ms and filter slope to 12 dB/octave. This turns out that the calculated noise accompanying the signal is

$$\sqrt{8.3375 \text{ Hz}} \times 4 \text{ nV} \times 1000 = 11.55 \ \mu\text{V}\sqrt{\text{Hz}}. \qquad (1)$$

Practically, in homogenous magnetic fields, the ME sensor exhibits a sensitivity of 307.4 mV/Oe and a background noise of ±10 μV (see Figs. 2(a) and 2(b), respectively).

C. Experimental setup

Measurement setup under investigation is presented in Fig. 3(a). A (inhomogeneous) magnetic field is generated from a small cylindrical permanent magnet of dimension 6 mm in diameter and 3 mm in height, which is placed in the sensor's xy-plane and at a distance of $y_o = 13$ mm from the sensor's center (see Fig. 3(b)). This permanent magnet creates a magnetic field along the z-axis perfectly perpendicular to the sensor plane (see Fig. 3(c)). Indeed, the magnetic field components (H_x, H_y, H_z) of magnet produced on the sensor surface along the x-axis were experimentally measured by using a Hall effect magnetometer (Magnetic Instrumentation, Inc., Model 2100 Gaussmeter) and shown in Fig. 4. It exhibits a maximum ($H_z = 60$ Oe) at the sensor center (i.e., at $x = 0$). For the whole range of the sensor length ($x = \pm 7.5$ mm), the magnetic field homogeneity ($\Delta H/H_{max}$) reaches the value of 75%. The magnetic field is almost perfectly annulled in the sensor plane.

The magnetic nanoparticles placed closely above the sensor surface are mainly magnetized by the magnetic field component H_z of the permanent magnet; however, its stray magnetic fields (h) distribute on the x-y sensor plane (Fig. 3(b)). The nanoparticles thus are enabled to be detected by the sensor.

In this investigation, experiments were performed using the chitosan-coated superparamagnetic Fe_3O_4 magnetic fluid with diameter of 50 nm contained in an Eppendorf safe-lock tube. During the measurement, the tube moves linearly
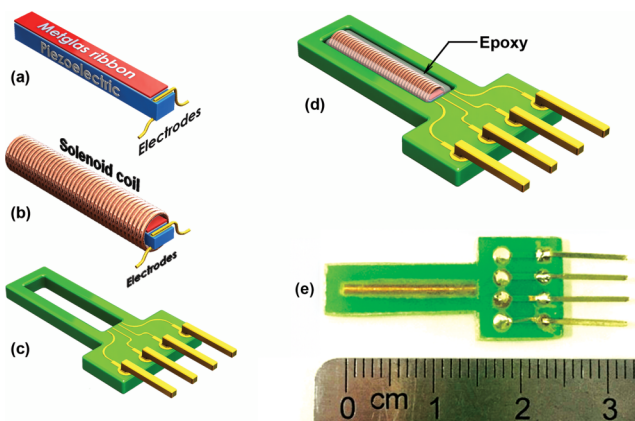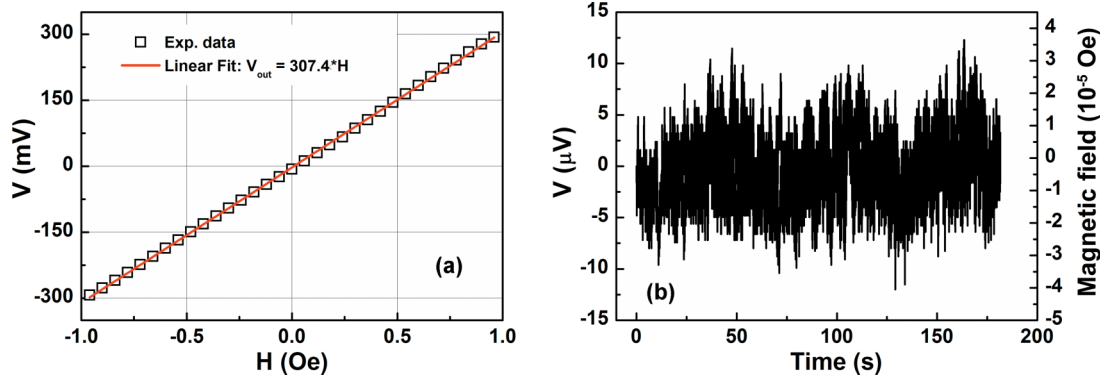
FIG. 2. The low magnetic field response (a) and background noise (b) of ME sensor measured by lock-in amplifier at the resonant frequency of f = 100 kHz and the quality factor (f/Δf) of 66.67.

along the sensor axis, thanks to an automatic mechanical system (Fig. 3(a)). The low rate of this motion was kept at 0.2 mm/s. The distance from the DC step motor was kept in the range of 1 m to the sensor to ensure that the magnetic field caused by the motor is not distributed to the system. For each measurement, an amount of 1 μl at a starting concentration of 50 μg/μl and diluted in 2× dilutions is determined and transferred to the tube by using a micropipettor. The height z_o was defined as the distance between the magnetic particles and the ME composite's surface inside the sensor (Fig. 3(b)).

III. RESULT AND DISCUSSION

A. Characterization of magnetic nanoparticles

The magnetic properties of magnetic nanoparticles were measured at room temperature by using the Lake Shore 7404 vibration sample magnetometer (VSM). The magnetic hysteresis loop is presented in Fig. 5 for 50 μg of iron oxide nanoparticles in 5 μl fluid volume. Clearly, the sample shows

superparamagnetic behavior with negligible coercivity and remanent magnetization (Fig. 5, inset). The saturation magnetization of these nanoparticles is approximately 17 emu/g. This value of the saturation magnetization is the same order as those from the reported results in literatures (16–33 emu/g).[20,21] From this curve, the magnetic susceptibility χ of magnetic nanoparticles is calculated to be ~0.03 at the applied magnetic field below 100 Oe.

B. On surface detection of magnetic nanoparticles

In this subsection, all experiments are carried out with z_o = 2 mm, i.e., in the configuration, the nanoparticles are placed closest to the sensor surface. The detection of nanoparticles is performed by recording the ME sensor signal during magnetic nanoparticles uniformly passing along the sensor axis. The obtained results are illustrated in Fig. 6(b) for 50 μg of iron oxide nanoparticles. It is clearly seen that the ME signal maximum does not reach when the magnetic particles pass the sensor's center, at which the magnetic field H created by the permanent magnet is maximal (Fig. 6(a)). The sensor signal, however, exhibits two peaks at x = −4 and +4 mm. These findings can be understood by considering the field distribution h produced by the magnetic particles on the ME laminate bar as described in Fig. 6(c). Indeed,
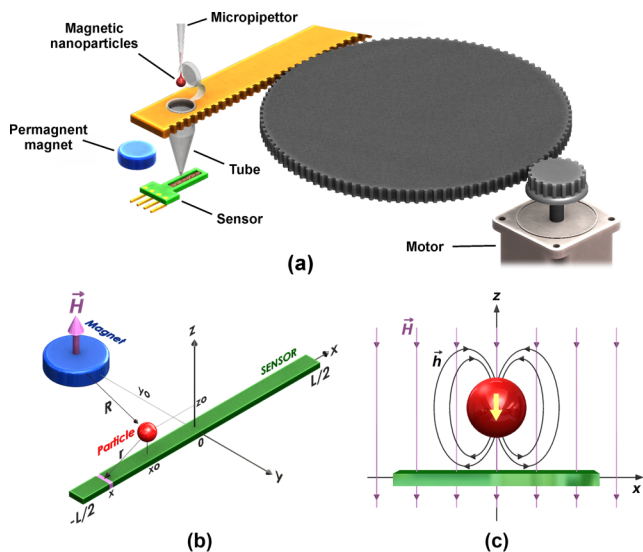
FIG. 3. The schematics of experimental setup for nanoparticle detection using ME sensor (a), the permanent magnet position with respect to the sensor (b), and magnetic fluxes created by permanent magnet and nanoparticles (c).
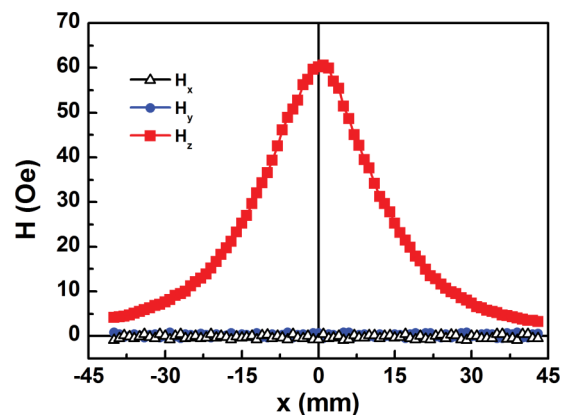
FIG. 4. Strength of the magnetic field components in-plane, along (Hx) and transversal (Hy) to the length and out-of-plane (Hz) of sensor supporting a magnetic field of the magnet perfectly perpendicular to the sensor plane (as illustrated in Fig. 3(c)).
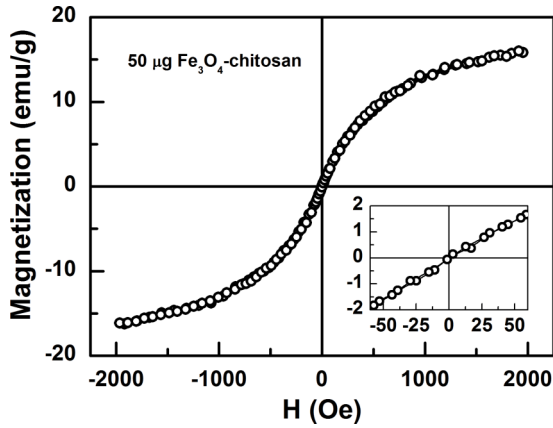
FIG. 5. Magnetic hysteresis loop of 5 μl fluid volume of Fe_3O_4-chitosan nanoparticles at the concentration of 50 μg/μl. The inset shows the region in small field range.

FIG. 6. Systematic understanding of ME sensor signal in detection of magnetic nanoparticles: (a) experimental and calculated data of ME sensor signals, (b) stray field distribution produced by nanoparticles placing at left, center, and right side of the sensor, and (c) shear-lag effect with the normal stress distribution along the sensor length.

when the particles were at the sensor's center (Fig. 6(c), center), the magnetic flux lines are perfectly symmetric with respect to the sensor's center but act in the opposite direction. The ME effects can occur at every local sensor positions, but their sum is annulled for the whole ME composite bar. When the particles passed through the center (Fig. 6(c), left or right), this symmetric distribution of the magnetic flux lines no longer exists, leading to the increase of the ME signal and the appearance of maximum peaks. The signal is reduced when the particles are far from the center due to the weakened magnetic field. Following these arguments, however, the ME signal peaks should occur at sensor's leftmost and rightmost (i.e., at $x = -7.5$ and $+7.5$ mm). A complete description for this phenomenon is given below, thanks to the calculation taking into account the shear-lag effect.

Let us consider nanoparticles as a magnetic dipole m, which is proportional to magnetized magnetic field H caused by the permanent magnet and mass of the particle m_g,

$$m = \chi \cdot m_g \cdot H. \tag{2}$$

For the experimental setup presented in Fig. 2(a), the stray field h was created at a point X(x,0,0) in the ME sensor by the magnetic dipole (placed at point P(x_o,0,z_o) which is at a distance r away from the point X) is approximated by the conventional Biot-Savart law,

$$\vec{h} = \frac{3\,(\vec{m}\vec{r})\,\vec{r}}{r^5} - \frac{\vec{m}}{r^3}. \tag{3}$$

The x-field component $h_x(x)$ is written by

$$h_x = \frac{3\chi m_g \mu z_o}{R^5}$$
$$\times \frac{2x_o(x - x_o)^2 + (x_o^2 + y_o^2 - 2z_o^2)(x - x_o) - x_o z_o^2}{\left\{(x - x_o)^2 + z_o^2\right\}^{\frac{5}{2}}}, \tag{4}$$

where μ are the vector quantities representing the magnetic moment of the magnet. The ME voltage (or sensor signal) can be calculated by integrating all of the contributions over the

area of the sensor length,

$$V_{out} = \int_{-L/2}^{L/2} dV_{out} = \int_{-L/2}^{L/2} k\,(x)\,h_x dx, \tag{5}$$

where $k(x)$ is conversion factor determined by the ME coefficient and other material parameters.

Although one can assume a constant value for the ME coefficient, the stress σ distribution might still be modified by shear-lag effects. For simplifying, here, one can apply a simple one-dimensional hyperbolic shear-lag equation,[22,23]

$$k\,(x) = A + B\sinh(Cx) + D\cosh(Cx). \tag{6}$$

In Eq. (6), the constants A, B, C, and D are determined by satisfying the boundary conditions that the strain $\sigma = \sigma_{max}$ at $x = 0$ and $\sigma = 0$ at $x = \pm L/2$ ($= \pm 7.5$ mm). Then, the conversion factor and/or the normalized stress distribution σ/σ_{max} is obtained as plotted in Fig. 6(d).

The ME-voltage can be determined by integrating Equation (5) with respect to the variable x with and without consideration of the shear-lag effect (i.e., Eq. (6)). The calculated ME sensor signals are shown in Fig. 6(b). It is clearly seen that by using the stray field distribution of magnetic nanoparticles as well as shear-lag effect, the experimental sensor signal is fully described.

The ME sensor signals recorded for different amounts of magnetic nanoparticles varied from 0.31 to 50 μg are illustrated in Fig. 7(a). It shown that the ME signal shapes
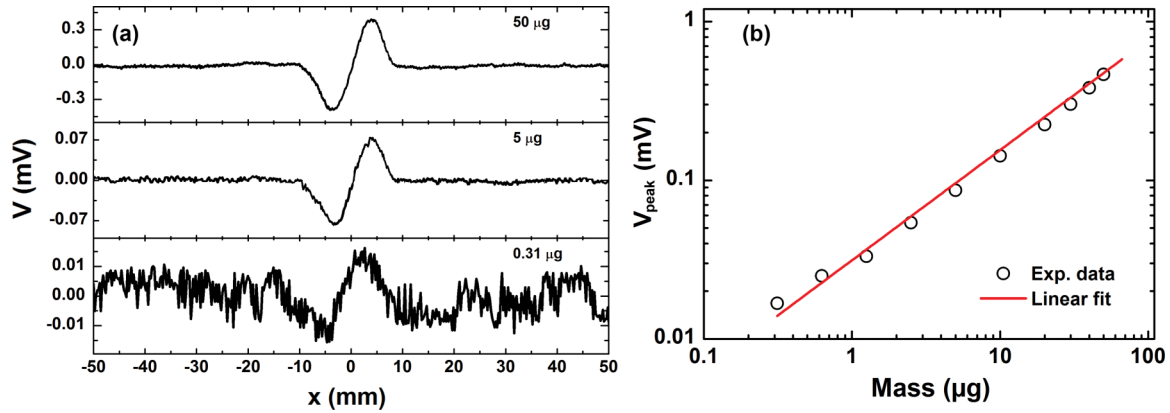
FIG. 7. The ME sensor signals recorded for different amounts of magnetic nanoparticles (a) and mass dependence of ME signal peak amplitude (b).
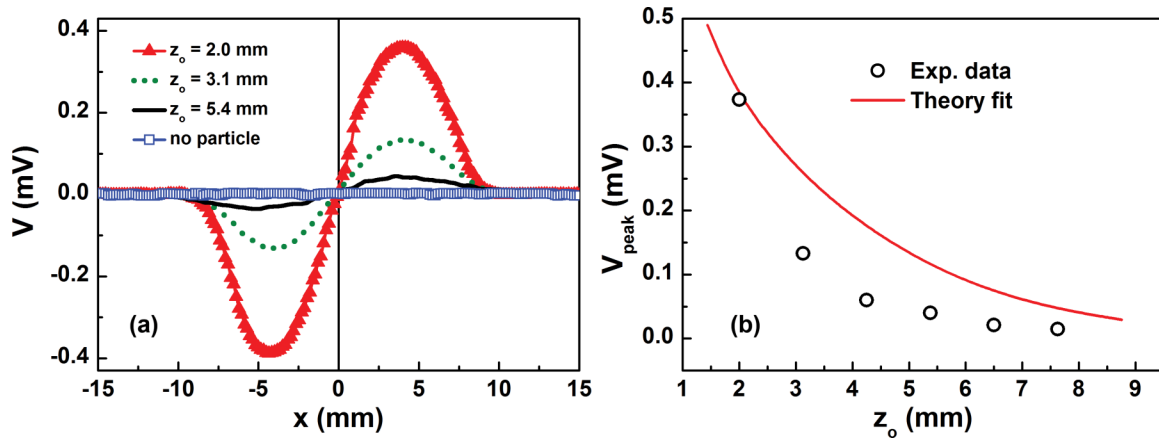
FIG. 8. Experimental ME sensor signals (a) and maximum value collected at $x = 4$ mm (b) measured at different height z_o position for the amount of 50 μg iron oxide.

closely resemble each other, where the maximum peaks always occur at $x = \pm 4$ mm. However, the amplitude of these peaks is proportional with the particle mass (Fig. 7(b)). Here, the smallest detectable amount of magnetic nanoparticles was estimated to be about 0.31 μg (corresponding to a magnetic moment of 5.4×10^{-7} emu). The mass dependence of the ME signal amplitude showed a linear behavior with a slope of 15 μV/μg. As already mentioned in Section II A and given in Fig. 2(b), the background noise of this experimental setup of about 10 μV that means the mass limit of detection of about 0.15 μg iron oxide, which corresponds to a detection limit of 2.7×10^{-7} emu. This is comparable with that reported earlier by Dong *et al.*[16] By developing an advanced measurement setup for noise level reduction, this ME sensor could be able to detect lower magnetic field levels.

C. Distance detection of magnetic nanoparticles

As regards the distance detection of magnetic nanoparticles, the ME sensor signals are recorded for 50 μg of iron oxide at different heights z_o. The observed results are presented in Fig. 8(a) for $z_o = 2$, 3.1, and 5.4 mm. The findings show that the signal shape is similar for measurements with $z_o \leq 8$ mm. The peaks also occur at $x = \pm 4$ mm and decreases exponentially with increasing z_o (Fig. 8(b)). The calculated results performed by Eqs. (5) and (6), however, exhibit a large

difference with experimental data at large distances z_o (from the sensor surface). A better fit must be performed taking into account the distance from the ME laminate surface. However, such accurate determination cannot be reached in this paper.

Note that, at $z_o = 7.6$ mm, the peak signal still reaches the value as high as 18 μV, i.e., almost double of magnitude higher than the detection limit. Further research is in progress to complete the description and to develop for the local detection of magnetic nanoparticles at a tissue depth.

IV. CONCLUSION

This paper presents a simple and cheap magnetic probe functioned on the basis of the ME effects for the purpose of distance detections of magnetic nanoparticles. For a system setup with the measurable minimum signal of 18 μV, the probe is able to monitor an iron oxide amount as low as 0.31 μg at the distance of 2 mm from the probe surface, which corresponds to a detection limit of 2.7×10^{-7} emu. To detect a spot with magnetic nanoparticles at a distance of about 7.6 mm, it should contain at least 50 μg of iron oxide. By developing an advanced measurement setup for noise level reduction, this ME sensor could be able to detect lower magnetic field levels. This is rather suitable approach for local detection of magnetic nanoparticles (MNPs) at a depth of several millimetres in the body during clinical interventions.

[1] P. P. Freitas, H. A. Ferreira, D. L. Graham, L. A. Clarke, M. D. Amaral, V. Martins, L. Fonseca, and J. S. Cabral, in *Magnetoelectronics*, edited by M. Johnson (Elsevier, Amsterdam, 2004).

[2] B. D. Tu, T. Q. Hung, N. T. Thanh, T. M. Danh, N. H. Duc, and C. G. Kim, "Planar Hall bead array counter microchip with NiFe/IrMn bilayers," J. Appl. Phys **104**, 074701 (2008).

[3] H. Kim, V. Reddy, K. Woo Kim, I. Jeong, X. H. Hu, and C. G. Kim, "Single magnetic bead detection in a microfluidic chip using planar hall effect sensor," J. Magn. **19**, 10 (2014).

[4] B. D. Tu, L. V. Cuong, T. Q. Hung, D. T. Huong Giang, T. M. Danh, N. H. Duc, and C. G. Kim, "Optimization of spin-valve structure NiFe/Cu/NiFe/IrMn for planar Hall effect based biochips," IEEE Trans. Magn. **45**, 2374 (2009).

[5] M. Visscher, S. Waanders, J. Pouw, and B. ten Haken, "Depth limitations for *in vivo* magnetic nanoparticle detection with a compact handheld device," J. Magn. Magn. Mater. **380**, 246 (2015).

[6] H. J. Hathaway, K. S. Butler, N. L. Adolphi, D. M. Lovato, R. Belfon, D. Fegan, T. C. Monson, J. E. Trujillo, T. E. Tessier, H. C. Bryant, D. L. Huber, R. S. Larson, and E. R. Flynn, "Detection of breast cancer cells using targeted magnetic nanoparticles and ultra-sensitive magnetic field sensors," Breast Cancer Res. **13**(5), R108 (2011).

[7] N. B. Othman, "Magnetic nanoparticle imaging for biomedical applications," Ph.D. thesis, Kyushu University, Japan, 2014.

[8] J. Joseph and V. Jayashankar, "Magnetic sensor for non-invasive detection of blood pulse and estimation of arterial compliance," in *2010 IEEE EMBS Conference on Biomedical Engineering & Sciences (IECBES 2010)* (IEEE, Kuala Lumpur, Malaysia, 2010), p. 175.

[9] L. T. Hien, L. K. Quynh, V. T. Huyen, B. D. Tu, N. T. Hien, D. M. Phuong, P. H. Nhung, D. T. H. Giang, and N. H. Duc, "DNA-magnetic bead detection using disposable cards and the anisotropic magnetoresistive sensor," Adv. Nat. Sci.: Nanosci. Nanotechnol. **7**, 045006 (2016).

[10] N. Pamme, "Magnetism and microfluidics," Lab Chip **6**, 24–38 (2006).

[11] I. Giouroudi and F. Keplinger, "Microfluidic biosensing systems using magnetic nanoparticles," Int. J. Mol. Sci. **14**(9), 18535–18556 (2013).

[12] D. J. B. Bechstein, J. R. Lee, C. C. Ooi, A. W. Gani, K. Kim, R. J. Wilson, and S. X. Wang, "High performance wash-free magnetic bioassays through microfluidically enhanced particle specificity," Sci. Rep. **5**, 11693 (2015).

[13] T. Takamura, P. J. Ko, J. Sharma, R. Yukino, S. Ishizawa, and A. Sandhu, "Magnetic-particle-sensing based diagnostic protocols and applications," Sensors **15**, 12983–12998 (2015).

[14] L. K. Quynh, B. D. Tu, D. X. Dang, D. Q. Viet, L. T. Hien, D. T. Huong Giang, and N. H. Duc, "Detection of magnetic nanoparticles using simple AMR sensors in Wheatstone bridge," J. Sci.: Adv. Mater. Devices **1**, 98 (2016).

[15] N. H. Duc and D. T. Huong Giang, "Multiferroic magneto-electrostrictive composites and applications," in *in Advanced Magnetism and Magnetic Materials*, edited by N. H. Duc (Vietnam National University Hanoi Press, 2015), Vol. 2.

[16] S. Dong, J. Zhai, N. Wang, F. Bai, J. F. Li, D. Viehland, and T. A. Lograsso, "Fe-Ga/PbMg$_{1/3}$Nb$_{2/3}$O$_3$–PbTiO$_3$ Magnetoelectric laminate composites," Appl. Phys. Lett. **87**, 222504 (2005).

[17] D. T. Huong Giang, P. A. Duc, N. T. Ngoc, and N. H. Duc, "Geomagnetic sensors based on Metglas/PZT laminates," Sens. Actuators, A **A179**, 78 (2012).

[18] D. T. Huong Giang, P. A. Duc, N. T. Ngoc, N. T. Hien, and N. H. Duc, "Enhancement of the magnetic flux in Metglas/PZT-magnetoelectric integrated 2D geomagnetic device," J. Magn. **17**, 308 (2012).

[19] D. T. Huong Giang, P. A. Duc, N. T. Ngoc, N. T. Hien, and N. H. Duc, "Spatial angular positioning device with three-dimensional magnetoelectric sensors," Rev. Sci. Instrum. **83**, 095006 (2012).

[20] G.-y. Lia, Y.-r. Jiangb, K.-l. Huang, P. Ding, and J. Chen, "Preparation and properties of magnetic Fe$_3$O$_4$-chitosan nanoparticles," J. Alloys Compd. **466**, 451 (2008).

[21] K. Donadel, M. D. V. Felisberto, V. T. Fávere, M. Rigoni, N. J. Batistela, and M. C. M. Laranjeira, "Synthesis and characterization of the iron oxide magnetic particles coated with chitosan biopolymer," Mater. Sci. Eng. C **28**, 509 (2008).

[22] C. M. Chang and G. P. Carman, "Modeling shear lag and demagnetization effects in magneto-electric laminate composites," Phys. Rev. B **76**, 134116 (2007).

[23] H. A. Salim and J. F. Davalos, "Shear lag of open and closed thin-walled laminated composite beams," J. Reinf. Plast. Compos. **24**, 673 (2005).